



SpoIVA-SipL Complex Formation Is Essential for *Clostridioides difficile* Spore Assembly

Megan H. Touchette,^{a*} Hector Benito de la Puebla,^a Priyanka Ravichandran,^b Aimee Shen^{a,b}

^aDepartment of Molecular Biology and Microbiology, Tufts University School of Medicine, Boston, Massachusetts, USA

^bDepartment of Microbiology and Molecular Genetics, University of Vermont, Burlington, Vermont, USA

ABSTRACT Spores are the major infectious particle of the Gram-positive nosocomial pathogen *Clostridioides difficile* (formerly *Clostridium difficile*), but the molecular details of how this organism forms these metabolically dormant cells remain poorly characterized. The composition of the spore coat in *C. difficile* differs markedly from that defined in the well-studied organism *Bacillus subtilis*, with only 25% of the ~70 spore coat proteins being conserved between the two organisms and with only 2 of 9 coat assembly (morphogenetic) proteins defined in *B. subtilis* having homologs in *C. difficile*. We previously identified SipL as a clostridium-specific coat protein essential for functional spore formation. Heterologous expression analyses in *Escherichia coli* revealed that SipL directly interacts with *C. difficile* SpoIVA, a coat-morphogenetic protein conserved in all spore-forming organisms, through SipL's C-terminal LysM domain. In this study, we show that SpoIVA-SipL binding is essential for *C. difficile* spore formation and identify specific residues within the LysM domain that stabilize this interaction. Fluorescence microscopy analyses indicate that binding of SipL's LysM domain to SpoIVA is required for SipL to localize to the forespore while SpoIVA requires SipL to promote encasement of SpoIVA around the forespore. Since we also show that clostridial LysM domains are functionally interchangeable at least in *C. difficile*, the basic mechanism for SipL-dependent assembly of clostridial spore coats may be conserved.

IMPORTANCE The metabolically dormant spore form of the major nosocomial pathogen *Clostridioides difficile* is its major infectious particle. However, the mechanisms controlling the formation of this resistant cell type are not well understood, particularly with respect to its outermost layer, the spore coat. We previously identified two spore-morphogenetic proteins in *C. difficile*: SpoIVA, which is conserved in all spore-forming organisms, and SipL, which is conserved only in the clostridia. Both SpoIVA and SipL are essential for heat-resistant spore formation and directly interact through SipL's C-terminal LysM domain. In this study, we demonstrate that the LysM domain is critical for SipL and SpoIVA function, likely by helping recruit SipL to the forespore during spore morphogenesis. We further identified residues within the LysM domain that are important for binding SpoIVA and, thus, functional spore formation. These findings provide important insight into the molecular mechanisms controlling the assembly of infectious *C. difficile* spores.

KEYWORDS *Clostridioides difficile*, *Clostridium difficile*, SipL, SpoIVA, coat assembly, spore formation

The Gram-positive pathogen *Clostridioides difficile* (formerly *Clostridium difficile*) is a leading cause of antibiotic-associated diarrhea and gastroenteritis in the developed world (1, 2). Since *C. difficile* is an obligate anaerobe, its major infectious particle is its aerotolerant, metabolically dormant spore form (3, 4). *C. difficile* spores in the environment are ingested by susceptible hosts and transit through the gastrointestinal tract until they sense specific bile salts in the small intestine that trigger spore germination

Citation Touchette MH, Benito de la Puebla H, Ravichandran P, Shen A. 2019. SpoIVA-SipL complex formation is essential for *Clostridioides difficile* spore assembly. *J Bacteriol* 201:e00042-19. <https://doi.org/10.1128/JB.00042-19>.

Editor Tina M. Henkin, Ohio State University

Copyright © 2019 Touchette et al. This is an open-access article distributed under the terms of the [Creative Commons Attribution 4.0 International license](https://creativecommons.org/licenses/by/4.0/).

Address correspondence to Aimee Shen, aimee.shen@tufts.edu.

* Present address: Megan H. Touchette, Nova Biomedical, Waltham, Massachusetts, USA.

Received 15 January 2019

Accepted 23 January 2019

Accepted manuscript posted online 28 January 2019

Published 26 March 2019

(5). The germinating spores outgrow into vegetative cells in the large intestine, which then produce the glucosylating toxins responsible for disease symptoms (6). A subset of these vegetative cells will initiate the developmental program of sporulation, producing the infectious spores needed for this organism to survive exit from the host (7, 8).

The basic architecture of spores is conserved across endospore-forming bacteria: a central core consisting of partially dehydrated cytosol is surrounded by a protective layer of modified peptidoglycan called the cortex, which is in turn encased by a series of proteinaceous shells known as the coat (9). The cortex is critical for maintaining spore dormancy and conferring resistance to heat and ethanol, while the coat acts as a molecular sieve that protects the spore from enzymatic and oxidative insults (9–11). The cortex is assembled on top of the thin layer of vegetative cell wall that is sandwiched between two membranes known as the inner forespore and outer forespore membranes. The outer forespore membrane derives from the mother cell and encases the developing forespore during engulfment by the mother cell. During this time, a series of self-polymerizing proteins will assemble on the outer forespore membrane and eventually form the concentric layers of protein that define the spore coat (10).

The mechanisms controlling coat assembly have been studied for decades in *Bacillus subtilis*, where the key coat-morphogenetic proteins that control the recruitment and assembly of the coat layers have been identified (10, 12). The innermost layer, known as the basement layer, is formed through the coordinated actions of SpoVM, SpoIVA, and SpoVID. SpoVM is a small amphipathic helix that embeds itself in the forespore membrane (13) and directly interacts with SpoIVA (14), facilitating SpoIVA's assembly around the forespore (14). SpoIVA is a self-polymerizing ATPase (15) that binds SpoVM through residues in SpoIVA's C-terminal region (14). In the absence of SpoVM, SpoIVA forms a single focus on the forespore and fails to encase the forespore (14, 16). SpoIVA also recruits SpoVID to the forespore (17), and the interaction of these proteins promotes the encasement of both around the forespore (17).

Loss of any one of these coat-morphogenetic proteins in *B. subtilis* prevents recruitment of additional coat proteins to the forespore and causes the polymerized coat to mislocalize to the mother cell cytosol, at least in the case of *spoIVA* (18) and *spoVID* (19) mutants. Loss of either SpoIVA or SpoVM prevents cortex assembly and, thus, results in a severe defect in heat-resistant spore formation ($\sim 10^{-8}$) due to activation of a quality control pathway conserved in the bacilli (18, 20, 21). In contrast, loss of SpoVID results in only an ~ 5 -fold defect in heat-resistant spore formation as well as lysozyme resistance (22), consistent with the *spoVID* mutant producing a detectable cortex layer (19).

Interestingly, while SpoIVA and SpoVM appear to be conserved in all spore-forming organisms, SpoVID is conserved only in the bacilli (23). Of the nine coat-morphogenetic proteins that have been defined in *B. subtilis*, only two have homologs in *C. difficile*, namely, SpoIVA and SpoVM (24). While we previously showed that SpoIVA is critical for spore formation in *C. difficile* (25), we surprisingly found that SpoVM is largely dispensable for functional *C. difficile* spore formation, despite abnormalities in coat adherence to the forespore being observed (26). Furthermore, unlike mutants of *B. subtilis*, both *spoVM* and *spoIVA* mutants in *C. difficile* produce cortex (25, 26) although some abnormalities in cortex thickness are observed (26).

Although SpoVID is not conserved in the clostridia, we previously showed that *C. difficile* produces a functional homolog to SpoVID called SipL (CD3567). Similar to *B. subtilis* SpoVID (17), *C. difficile* SipL is required for proper localization of the coat around the forespore (25), and SipL directly interacts with *C. difficile* SpoIVA (25) even though SipL and SpoVID exhibit no sequence homology outside their shared C-terminal LysM domains (25) (Fig. 1A). However, *C. difficile*'s SipL LysM domain directly binds to SpoIVA (25), whereas SpoVID's LysM domain is dispensable for SpoVID binding to SpoIVA in *B. subtilis* (17). Furthermore, loss of *C. difficile* SipL causes a severe heat resistance (HR)

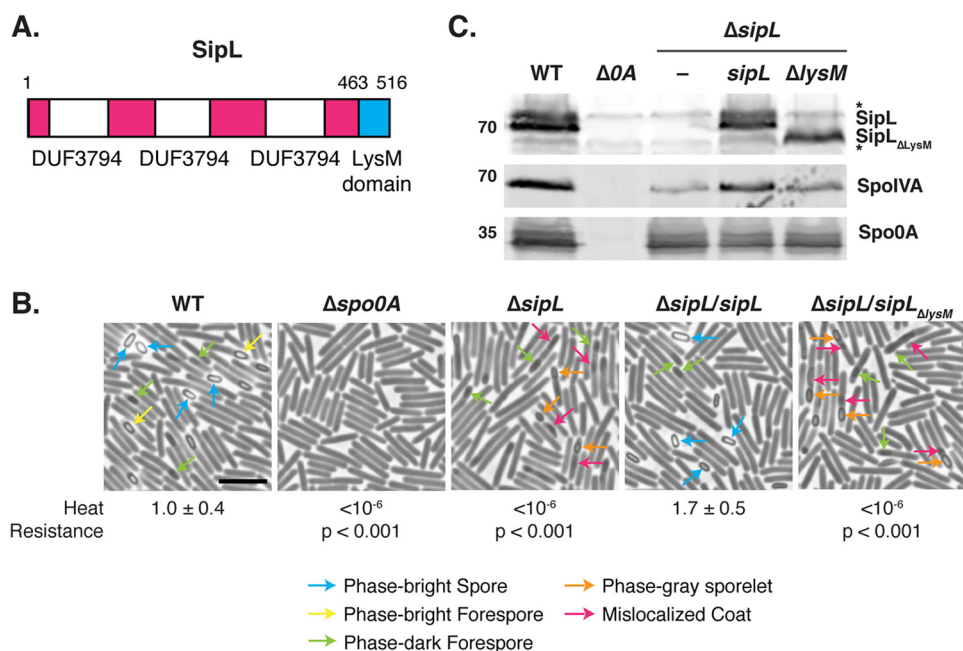


FIG 1 The LysM domain of *C. difficile* is essential for spore formation. (A) Schematic of *C. difficile* SipL domain structure. SipL contains three domains of unknown function (DUF3794) and a C-terminal LysM domain. (B) Phase-contrast microscopy analyses of the indicated *C. difficile* strains ~20 h after sporulation induction. The $\Delta sipL$ strain was complemented with either the wild-type allele or one encoding a deletion of the LysM domain ($\Delta sipL/sipL_{\Delta lysM}$ strain). Arrows mark examples of sporulating cells at different stages of maturation: blue arrows highlight phase-bright free spores; yellow arrows mark mature phase-bright forespores, which are formed following cortex formation (22, 24); green arrows highlight immature phase-dark forespores; orange arrows highlight phase-gray sporelets, which produce a phase-dark ring surrounding the forespore but do not become phase-bright; and pink arrows demarcate regions suspected to be mislocalized coat based on previous studies (26, 30). Heat resistance efficiencies were determined from 20- to 24-h sporulating cultures and represent the mean and standard deviation for a given strain relative to the level of the wild type based on a minimum of three independent biological replicates. Statistical significance relative to the level of the wild type was determined using a one-way ANOVA and Tukey's test. Scale bar, 5 μ m. The limit of detection of the assay is 10⁻⁶. (C) Western blot analyses of SipL, SpoIVA, and Spo0A. SipL was detected using an antibody raised against SipL lacking its LysM domain (i.e., SipL _{Δ lysM}). Asterisks indicate nonspecific bands detected by the SipL _{Δ lysM} antibody. SpoIVA levels were analyzed because of the prior finding that SpoIVA levels are reduced in the absence of SipL (25). Modest decreases in SipL levels were observed in the $\Delta sipL$ and $\Delta sipL/sipL_{\Delta lysM}$ strains. Spo0A was used as a proxy for measuring sporulation induction (4, 25). The Western blots shown are representative of the results of three independent biological replicates.

defect (<10⁻⁶) (25), in contrast with the mild defects observed in *B. subtilis spoVID* mutants (19, 22).

While we previously showed that SipL's LysM domain is sufficient to mediate binding to SpoIVA using a heterologous *Escherichia coli* expression system (25), in this study we tested the hypothesis that this interaction is critical for *C. difficile* spore formation using deletion and coimmunoprecipitation analyses in *C. difficile*. We also identified residues in the LysM domain important for both SipL function and binding to SpoIVA. Last, we determined the requirement for the LysM domain to localize SipL to the forespore and the localization dependencies of SpoIVA and SipL.

RESULTS

The LysM domain is required for SipL function. Based on our prior finding that SipL binding to SpoIVA depends on SipL's LysM domain when it is heterologously produced in *E. coli* (25), we sought to test whether SipL binding to SpoIVA is critical for SpoIVA and/or SipL function during *C. difficile* sporulation. To this end, we expressed a construct encoding a deletion of the LysM domain in a $\Delta sipL$ strain that we previously constructed (27) to generate a $\Delta sipL/sipL_{\Delta lysM}$ strain. As with all constructs reported in this paper, the $sipL_{\Delta lysM}$ construct was expressed from the native *sipL* promoter from the ectopic *pyrE* locus of the 630 Δerm background using the *pyrE*-based allele-coupled

exchange (ACE) system (28). Functional spore formation in the *sipL* _{Δ lysM} and wild-type *sipL* complementation strains was then assessed using a heat resistance assay. In this assay, sporulating cultures are heat treated to kill vegetative cells, while heat-resistant spores in the cultures capable of germinating and forming colonies on plates are enumerated and compared to CFU counts from untreated samples. The LysM domain mutant (Δ lysM strain) was defective in heat-resistant spore formation at levels similar to those of the parental Δ sipL strain (~6-log-unit decrease) (Fig. 1B). In contrast, the wild-type *sipL* construct expressed from the *pyrE* locus (Δ sipL/*sipL* strain) fully complemented the parental Δ sipL strain.

To ensure that the inability of the *sipL* _{Δ lysM} construct to complement the Δ sipL strain was not due to destabilization of SipL _{Δ lysM}, we analyzed SipL levels in the different *sipL* complementation strains using an antibody raised against SipL lacking its LysM domain. These analyses revealed that loss of the LysM domain did not reduce SipL levels in sporulating cells relative to levels of the wild-type or the wild-type *sipL* complementation strain (Fig. 1C). Thus, the sporulation defect of the Δ sipL/*sipL* _{Δ lysM} strain is because SipL lacking its LysM domain is nonfunctional. Consistent with our prior finding that SipL helps stabilize SpoIVA (25), SpoIVA levels were slightly reduced in the Δ sipL and Δ sipL/*sipL* _{Δ lysM} strains. However, the reduction in SpoIVA levels did not appear as large or as consistent in our analyses of the 630 Δ erm Δ sipL mutants relative to levels of the previously characterized JIR8094 *sipL::erm* Targetron mutant (25), which may reflect strain-specific differences between JIR8094 and 630 Δ erm (29).

Phase-contrast microscopy analyses revealed that the Δ lysM strain resembled the Δ sipL strain in that it failed to produce phase-bright spores (Fig. 1B). Instead, these defective strains occasionally produced phase-gray sporelets (Fig. 1B, orange arrows) (20) that did not achieve the oval shape and phase-bright contrast of wild-type spores. Furthermore, phase-dark regions (Fig. 1B, pink arrows) were visible in the mother cell cytosol of the Δ lysM and Δ sipL strains but not in the wild type and the wild-type complementation strain. These regions likely correspond to mislocalized spore coat based on prior work (25, 26, 30). To address this possibility, we visualized the spore coat of these strains using transmission electron microscopy (TEM). The Δ sipL/*sipL* _{Δ lysM} and Δ sipL cells failed to localize coat around the forespore in analyses of >50 sporulating cells. Instead, polymerized coat detached from the forespore and mislocalized to the mother cell cytosol in ~40% of these cells (Fig. 2, pink arrowhead), while polymerized coat appeared to slough off the forespore (previously termed “bearding” [26]) (Fig. 2, yellow arrowhead) in ~40% of these strains. Neither of these phenotypes was detected in the wild type or the wild-type *sipL* complementation strain, where coat was localized around the forespore in ~95% of wild-type and Δ sipL/*sipL* cells or otherwise was not yet visible. Taken together, these analyses indicate that loss of SipL’s LysM domain results in coat mislocalization and impairs its adherence to the forespore.

SipL’s LysM domain mediates SipL binding to SpoIVA during *C. difficile* sporulation. Since we previously showed that SipL’s C-terminal LysM domain is sufficient to mediate binding to SpoIVA when it is recombinantly produced in *E. coli* (25, 31), we next wanted to confirm that the LysM domain mediates binding to SpoIVA in *C. difficile*. To this end, we compared the abilities of C-terminally FLAG-tagged SipL and SipL _{Δ lysM} to coimmunoprecipitate SpoIVA in sporulating *C. difficile* lysates. In particular, we complemented a Δ sipL strain with constructs encoding either wild-type SipL or SipL _{Δ lysM} carrying three copies of a C-terminal FLAG epitope tag (3 \times FLAG). FLAG-tagged wild-type SipL readily pulled down SpoIVA from sporulating cell lysates, whereas FLAG-tagged SipL _{Δ lysM} failed to pull down SpoIVA (Fig. 3). SpoIVA also did not coimmunoprecipitate with untagged SipL variants. Importantly, FLAG-tagged SipL fully restored functional spore formation to the Δ sipL background, whereas the FLAG-tagged SipL _{Δ lysM} failed to complement the Δ sipL strain (see Fig. S1 in the supplemental material). Taken together, these analyses imply that SipL binding to SpoIVA depends on SipL’s LysM domain in *C. difficile* and that this interaction appears essential for functional spore formation.

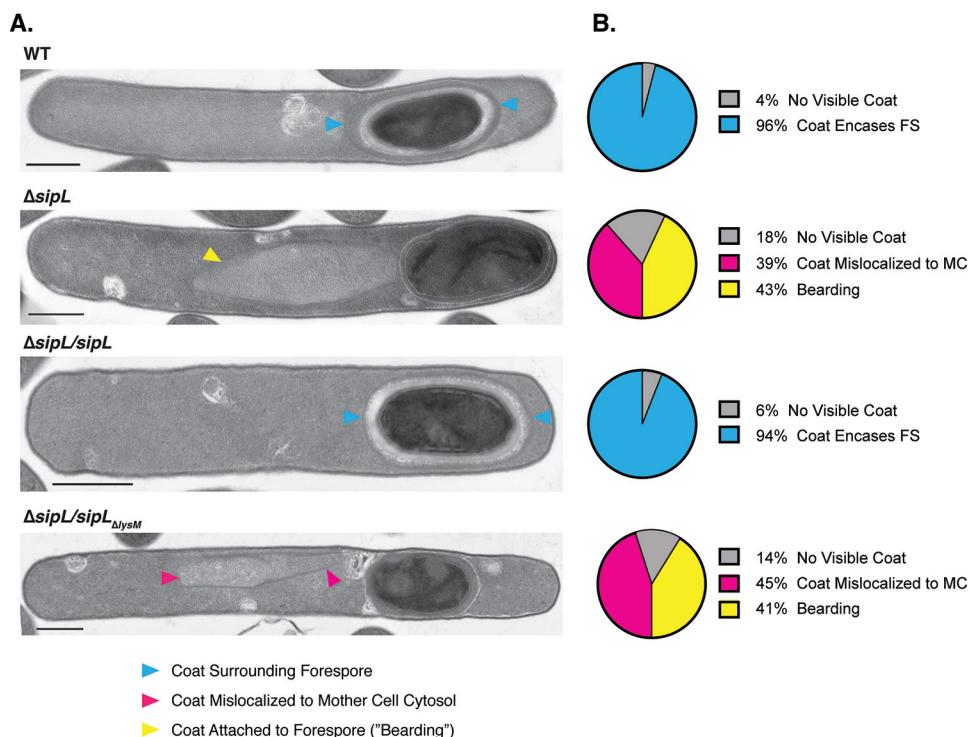


FIG 2 Loss of SipL’s LysM domain results in coat mislocalization defects. (A) Transmission electron microscopy (TEM) analyses of wild-type 630 Δerm , $\Delta sipL$, and $\Delta sipL$ strain complemented with either wild-type *sipL* or *sipL* encoding an LysM deletion (*sipL_{ΔlysM}*) after 23 h of sporulation induction. Scale bars, 500 nm. Blue arrowheads mark properly localized coat, i.e., surrounding the entire forespore (FS), whereas pink arrowheads mark coat that has completely detached from the forespore and is found exclusively in the mother cell (MC) cytosol. Yellow arrowheads mark cells where coat appears to be detaching from the forespore but remains partially associated, also known as “bearding” (26). (B) The percentages shown are based on analyses of at least 50 cells for each strain with visible signs of sporulation from a single biological replicate.

Clostridial SipL_{LysM} domains can functionally substitute for the *C. difficile* SipL_{LysM} domain. We next sought to identify key residues within SipL’s LysM domain that are required for the SpoIVA-SipL interaction and, thus, SipL function. To facilitate the identification of these residues, we tested whether LysM domains from closely related clostridial SipL homologs and SipL’s functional homolog, *B. subtilis* SpoVID (17, 25, 32), could replace the *C. difficile* SipL_{LysM} domain (Fig. 4A). Constructs encoding LysM domain chimeras from *Paraclostridium sordellii* and *Paraclostridium bifermentans* SipL homologs (~60% identity and 80% similarity with the *C. difficile* SipL_{LysM} domain), *Clostridium perfringens* SipL (39% identity and 57% similarity), and *B. subtilis* SpoVID (23% identity but 55% similarity) were constructed and used to complement a *C. difficile* $\Delta sipL$ strain. *P. sordellii* and *P. bifermentans* are members of the same *Peptostreptococcaceae* family as *C. difficile* (33) but part of a different genus (34), while *C. perfringens* is part of the *Clostridium* genus in the *Clostridiaceae* family.

$\Delta sipL$ strains complemented with the clostridial chimeras ($\Delta sipL/sipL-lysM_{bif}$, $\Delta sipL/sipL-lysM_{sor}$, and $\Delta sipL/sipL-lysM_{per}$ strains expressing the *lysM* genes from *P. bifermentans*, *P. sordellii*, and *C. perfringens*, respectively) were indistinguishable from the wild type and the wild-type *sipL* complementation strain ($\Delta sipL/sipL$ strain) by phase-contrast microscopy, since a mixture of phase-bright spores (blue arrows) and phase-bright (yellow arrows) and phase-gray (green arrows) forespores was visible in all strains producing clostridial LysM domains (Fig. S2A). In contrast, the *B. subtilis* chimera resembled the $\Delta sipL/sipL_{\Delta lysM}$ strain, with no phase-bright spores being detected and with most of the forespores being phase-dark or phase-gray sporelets (Fig. S2A, orange arrows). Similar to the parental $\Delta sipL$ strain, mislocalized coat was visible in the cytosol of the *B. subtilis* LysM chimera strain (Fig. S2A, pink arrows).

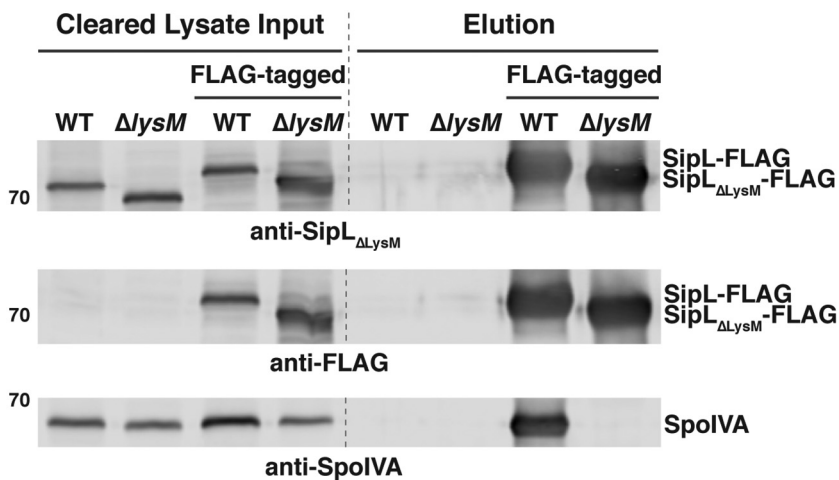


FIG 3 The LysM domain is required for SipL to bind SpoIVA in sporulating *C. difficile* cultures. FLAG-tagged SipL was immunoprecipitated from cleared lysates prepared from the indicated *C. difficile* $\Delta sipL$ complementation cultures (Input fraction) using anti-FLAG magnetic beads. Proteins bound to the beads after several washes were eluted using FLAG peptide (Elution fraction). WT refers to the $\Delta sipL$ strain complemented with the wild-type *sipL* allele; $\Delta lysM$ refers to the $\Delta sipL$ strain complemented with a *sipL* _{$\Delta lysM$} construct. FLAG-tagged indicates that the complementation constructs encode a C-terminal FLAG tag consisting of three successive FLAG tags, which resulted in the SipL-FLAG fusions exhibiting a higher mobility during SDS-PAGE. The untagged *sipL* complementation strains served as negative controls to ensure that untagged SipL and SpoIVA were not nonspecifically pulled down by the anti-FLAG beads. Sporulation was induced for 24 h before lysates were prepared. The immunoprecipitations shown are representative of three independent biological replicates.

Consistent with these observations, the clostridial SipL_{LysM} domain swap constructs fully complemented the $\Delta sipL$ strain in heat resistance assays (Fig. 4A and Fig. S2A), whereas the *B. subtilis* LysM chimeric strain, similar to the parental $\Delta sipL$ strain, failed to produce heat-resistant spores. Importantly, Western blotting revealed that the different chimeric SipL variants were produced at levels relatively similar to those of *C. difficile* SipL using an antibody raised against SipL _{$\Delta lysM$} (Fig. S2B) although slightly lower levels of SipL carrying the *B. subtilis* SpoVID LysM domain were observed. Taken together, these results suggest that clostridial SipL_{LysM} domains can still bind *C. difficile* SpoIVA, whereas the *B. subtilis* SpoVID_{LysM} domain cannot.

Identification of *C. difficile* LysM domain residues important for SipL function.

We next used these observations to guide finer-scale chimeric analyses of the *C. difficile* LysM domain by identifying differences between the sequences of the clostridial SipL_{LysM} domains and the *B. subtilis* SpoVID LysM domain. Clostridial LysM domains exhibited the greatest sequence similarity in the N-terminal portion of the LysM domain, so we swapped the residues corresponding to residues 463 to 482 of *C. difficile*'s SipL_{LysM} domain with those of the *B. subtilis* SpoVID LysM domain (Fig. 4A, region A). We also assessed the importance of the C terminus of the LysM domain by swapping out residues 483 to 516 (region E). While the C-terminal chimeric construct, *sipL*₄₈₃₋₅₁₆, fully complemented the $\Delta sipL$ strain, the *sipL*₄₆₃₋₄₈₂ chimeric construct resulted in an $\sim 3,000$ -fold decrease in heat resistance efficiency relative to that of the wild type and of the wild-type *sipL* complementation construct (Fig. 4B) ($P < 0.001$). Given the apparent importance of region A, we generated constructs encoding smaller-scale swaps, namely, residues 463 to 476 (region B), 475 to 476 (region C), and 478 to 480 (region D). Swapping the residues in regions B and C resulted in an ~ 100 -fold decrease in heat resistance efficiency relative to that of the wild type, while the region D swap construct resulted in an ~ 20 -fold decrease relative to that of the wild-type (Fig. 4B) ($P < 0.01$). Importantly, all of the SipL chimeric variants generated produced SipL at wild-type or close to wild-type levels (Fig. 4B), consistent with our earlier analyses of the $\Delta lysM$ strain (Fig. 1C).

Based on these findings, we next constructed individual point mutations in regions C and D. Region C comprises residues Trp475 and Asn476 in *C. difficile* SipL, which are

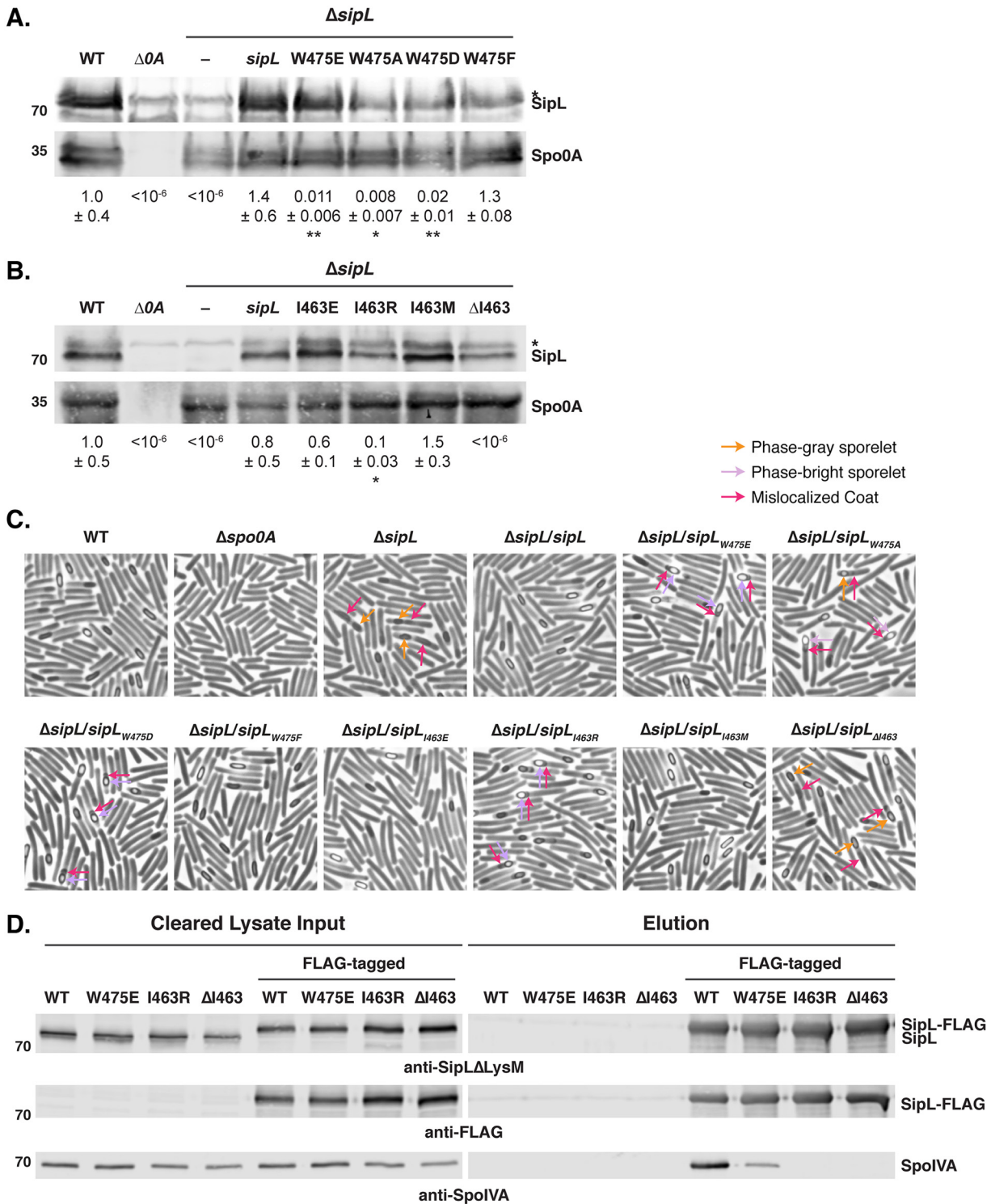


FIG 5 Identification of LysM domain residues required for optimal SipL function. (A and B) Western blot analyses of strains encoding SipL point mutations in Trp475 (A) and Ile463 (B) using an antibody raised against SipL lacking the LysM domain. The asterisk marks the nonspecific band detected by the anti-SipL Δ LysM antibody. Spo0A was used as a proxy for measuring sporulation induction (4, 25). The Western blots shown are representative of the results of three independent biological replicates. Heat resistance efficiencies were determined from 20- to 24-h sporulating cultures and represent the mean and standard deviation for a given strain relative to the level of the wild type based on a minimum of three independent biological replicates. The limit of detection of the assay is 10⁻⁶. Statistical significance relative to the level of the wild type was determined using one-way ANOVA and Tukey's test. **, *P* < 0.01; *, *P* < 0.05. (C) Phase-contrast microscopy analyses of the indicated *C. difficile* strains ~20 h after sporulation induction. The *ΔsipL* strain was complemented with either the wild-type allele or the indicated LysM domain mutations. Arrows mark examples of sporulating cells with various defects in maturation: orange arrows highlight phase-gray sporelets (20), which produce a phase-dark ring surrounding the forespore but do not become phase bright; purple arrows highlight phase-bright sporelets that appear

(Continued on next page)

To further assess the importance of the Trp475 residue for *C. difficile* SipL function, we mutated this residue to the small, uncharged residue, alanine (W475A), and the neutral, aromatic residue, phenylalanine (W475F). We also tested whether reducing the size of the negatively charged residue by introducing an aspartate at residue 475 instead of a glutamate would affect SipL function. While the conservative change, W475F, did not reduce SipL function, both the W475A and W475D mutations decreased heat-resistant spore formation to levels similar to the level of the W475E mutant (Fig. 5A). Since these strains also produced phase-bright sporelets and partially displaced coat (Fig. 5C), similar to the W475E mutant, these results suggest that the aromatic nature of Trp475 is critical to its function.

We next tested whether a single point mutation in region D, which consists of the three residues from 478 to 480, could recapitulate the ~20-fold decrease in heat resistance observed for the region D swap mutant relative to the resistance level of the wild type (Fig. 4). We focused on lysine 479 in *C. difficile* LysM, since this residue is a lysine in clostridial SipL_{LysM} domains but a negatively charged glutamate residue in the *B. subtilis* SpoVID LysM domain, and the other two residues in this region carried more conservative changes of alanine 478 to cysteine and of lysine 480 to arginine. Substitution of lysine 479 with glutamate did not impair the ability of this allele to complement a $\Delta sipL$ strain (K479E) (Fig. S3), suggesting that the other changes in region D could be responsible for the ~20-fold defect observed with this chimeric mutant. However, since the defect was relatively mild compared to that of the region B mutant, we did not further analyze point mutants in this region.

To assess whether additional residues in region B (463 to 482) might also contribute to SipL function, we constructed the following point mutant alleles based on differences between the LysM domains of *C. difficile* SipL and *B. subtilis* SpoVID: Y466C, G471E, and N482E. We also tested a few other residues just outside region B: T483I and E485S. These mutant constructs all fully complemented the $\Delta sipL$ strain (Fig. S3), suggesting that these individual residues do not affect SipL binding to SpoIVA.

We next analyzed the contribution of the first residue of *C. difficile*'s SipL_{LysM} domain because two observations suggested that Ile463 may be important for SipL binding to SpoIVA. Although SipL's LysM domain is annotated in the NCBI as spanning residues 464 to 508, we previously observed that a His-tagged construct encoding residues 464 to 516 failed to bind SpoIVA in coaffinity purification analyses in *E. coli*, whereas a construct spanning residues 463 to 516 resulted in robust pulldown (25). Furthermore, when we tested LysM chimeras using the NCBI-annotated LysM domains of clostridial SipL homologs, all of these constructs failed to complement the $\Delta sipL$ strain (data not shown). However, inclusion of the equivalent Ile463 residue allowed for full complementation (Fig. 4A). Taken together, these observations strongly suggest that Ile463 is important for SipL function.

Since Ile463 is a methionine in *B. subtilis* SpoVID, we tested whether the identity and/or precise position of residue 463 is critical for SipL function. Specifically, we generated complementation constructs in which Ile463 was either deleted ($\Delta I463$) or mutated to *B. subtilis* SpoVID's methionine (I463M), negatively charged glutamate (I463E), or positively charged arginine (I463R). No heat-resistant spores were detected when Ile463 was deleted (Fig. 5B), consistent with our observations with the chimeric LysM constructs (data not shown). In contrast, $sipL_{I463M}$, the *B. subtilis* SpoVID LysM point mutation, fully complemented the $\Delta sipL$ mutant (Fig. 5B). These results indicate that the sequence difference at residue 463 between the *C. difficile* and *B. subtilis* LysM domains is not responsible for the failure of the SpoVID LysM domain to complement for SipL function. Similarly, only a slight decrease in heat-resistant spore formation was

FIG 5 Legend (Continued)

swollen but are outlined by a phase-dark ring; and pink arrows demarcate regions likely to be mislocalized coat (26, 30). The images shown derive from two separate experiments, with the Trp475 and Ile463 variants being performed on different days. (D) Coimmunoprecipitations of FLAG-tagged SipL variants carrying either point mutations in the LysM domain (W475E or I463R) or lacking residue Ile463 ($\Delta I463$). Strains containing untagged SipL were used as negative controls to assess the specificity of the SpoIVA coimmunoprecipitations.

observed with the *sipL*_{I463E} mutation (Fig. 5B). In contrast, the *sipL*_{I463R} mutation decreased spore formation by ~9-fold ($P < 0.03$) (Fig. 5B), indicating that a large, positively charged residue at position 463 can impair SipL function.

Phase-contrast microscopy analyses revealed that the I463R mutant, similar to the W475 mutants, produced phase-bright sporelets and partially displaced coat (Fig. 5C), a phenotype that appears to be less severe than loss of SipL or the LysM domain altogether (Fig. 1B and Fig. S2). Indeed, the *sipL*_{ΔI463} strain resembled the parental $\Delta sipL$ strain in that only phase-gray sporelets (Fig. 5C, purple arrows) were observed, and the coat displacement appeared more severe than that of the W475 and I463R point mutant strains (pink arrows). Taken together, our results suggest that the spacing of the LysM domain, i.e., starting at position 463, is critical for SipL function, while the chemical identity of the residue at this position can also impact SipL function.

Isoleucine 463 and tryptophan 475 enhance binding of SipL to SpoIVA. The decreased ability of *sipL* constructs encoding mutations in either Ile463 or Trp475 to complement $\Delta sipL$ implied that point mutations in these residues decrease SipL binding to SpoIVA. To test this hypothesis, we generated constructs encoding FLAG-tagged SipL that carry mutations in these residues and measured their ability to pull down SpoIVA in coimmunoprecipitation analyses. Whereas SpoIVA was readily pulled down by FLAG-tagged wild-type SipL, no SpoIVA was detected in immunoprecipitations with SipL variants where Ile463 was either deleted ($\Delta I463$) or mutated to arginine (I463R) (Fig. 5D). Reduced amounts of SpoIVA were pulled down with the FLAG-tagged SipL_{W475E} variant relative to the level of the wild type. Interestingly, the pulldown results did not entirely match the severity of the mutations since the *sipL*_{W475E} allele resulted in an ~100-fold heat resistance defect, but the *sipL*_{I463R} allele caused only an ~9-fold heat resistance defect. This result suggests that even though SpoIVA can bind SipL_{W475E}, the interaction does not result in optimal SpoIVA and/or SipL function.

SipL localization to the forespore depends on the LysM domain. Since SpoIVA binding to SipL's LysM domain appears critical for these proteins to mediate spore formation, we hypothesized that SipL's LysM domain would be important for recruiting SipL to the forespore and allowing it to encase the forespore. To directly test this hypothesis, we complemented the $\Delta sipL$ strain with a construct encoding an mCherry fusion to SipL_{ΔLysM}. Whereas wild-type SipL fused to mCherry encases the forespore (Fig. 6A) as previously reported (27), deletion of the LysM domain prevented SipL_{ΔLysM}-mCherry localization to the forespore, since the SipL_{ΔLysM}-mCherry signal was largely distributed in the mother cell cytosol (Fig. 6A). Western blot analyses revealed that mCherry was not liberated from SipL_{ΔLysM}-mCherry (Fig. S4A), indicating that SipL's LysM domain directs SipL to the forespore and allows it to encase the forespore, presumably through its interaction with SpoIVA.

SipL requires SpoIVA to localize to and encase the forespore, while SpoIVA requires SipL to encase the forespore. To directly assess whether SpoIVA was required for SipL to localize to the forespore, we analyzed the localization of SipL-mCherry in a $\Delta spoIVA \Delta sipL$ mutant. It was necessary to use the double mutant because the presence of wild-type (untagged) SipL results in some SipL-mCherry being redistributed to the cytosol (data not shown). In the absence of SpoIVA, the SipL-mCherry signal was entirely cytosolic, a localization similar to the pattern of SipL_{ΔLysM}-mCherry (Fig. 6A), although the cytosolic SipL-mCherry signal appeared more intense in the absence of SpoIVA.

Since these results indicated that SipL localization to and around the forespore depends on SpoIVA through its interaction with SipL's LysM domain, we next assessed whether SpoIVA's localization around the forespore (26) depends on SipL. To test this question, we analyzed the localization of mCherry-SpoIVA, which has almost wild-type function (26), in the absence of SipL. For these experiments, mCherry-SpoIVA localization was analyzed in the presence of wild-type SpoIVA because mCherry-SpoIVA exhibits reduced encasement of the forespore if it is the only variant of SpoIVA present (26). While mCherry-SpoIVA encased the forespore (with some cytosolic localization)

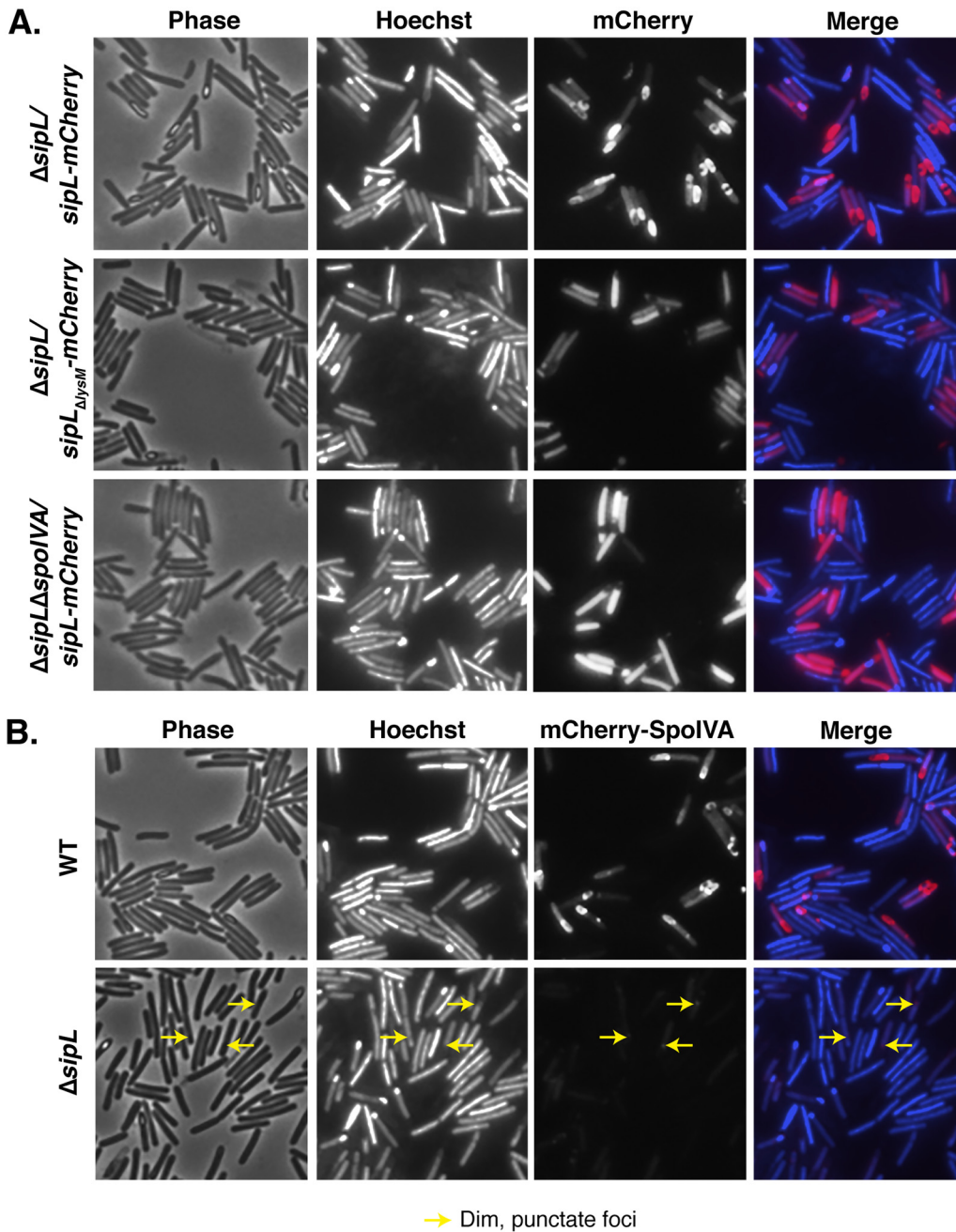


FIG 6 SipL binding to SpoIVA is required to localize SipL to the forespore, while SpoIVA encasement of the forespore depends on SipL. (A) Fluorescence microscopy analyses of either the $\Delta sipL$ or $\Delta sipL \Delta spoIVA$ strain complemented with constructs encoding either SipL-mCherry or SipL_{ΔlysM}-mCherry at 20 to 23 h post-sporulation induction. (B) mCherry-SpoIVA localization in either the wild-type or $\Delta sipL$ strain background. A wild-type copy of *spoIVA* was present in both strains because the fusion protein does not efficiently encase the forespore unless a wild-type copy of *spoIVA* is present (26). Cells were visualized using phase-contrast (phase) microscopy, and the nucleoid was visualized using Hoechst staining (48). The Hoechst-stained nucleoid is shown in blue, and mCherry fluorescence is shown in red. Hoechst stains the forespore brightly because the chromosome is compacted in the forespore. Engulfment completion excludes Hoechst from staining the forespore (48). The merge of Hoechst and mCherry staining is also shown. Arrows mark single, dim foci of mCherry-SpoIVA observed in the $\Delta sipL$ strain background. The images shown are representative of three independent biological replicates.

when produced in a wild-type strain background, mCherry-SpoIVA produced in the absence of SipL localized to a single, albeit dim, focus on the forespore at the mother cell proximal side (Fig. 6B). Notably, the amount of mCherry-SpoIVA produced in the $\Delta sipL$ background was reduced relative to that of the wild-type background (Fig. S4),

consistent with our original finding that SpoIVA levels are reduced in the absence of SipL (25). Taken together, our results indicate that SpoIVA-SipL binding is needed not only to bring SipL to the forespore but also for SipL to encase the forespore; in contrast, SpoIVA can find the forespore in the absence of SipL, but SpoIVA requires SipL to surround the forespore.

DISCUSSION

In this study, we show that the LysM domain of *C. difficile* SipL is critical for functional spore formation because it binds to SpoIVA and allows both of these proteins to encase the developing forespore. Our conclusions are based on the following observations: (i) SipL-mCherry mislocalizes to the cytosol if either SpoIVA or SipL's LysM domain is absent (Fig. 6); (ii) deletion of the LysM domain results in coat mislocalization to the mother cell cytosol (Fig. 2) and prevents heat-resistant spore formation (Fig. 1), analogous to the result with the *sipL* deletion mutant, and SpoIVA cannot bind to SipL Δ_{LysM} in immunoprecipitation analyses (Fig. 3); (iii) specific point mutations in SipL's LysM domain impair binding to SpoIVA and reduce functional spore formation (Fig. 5).

Through chimeric LysM analyses that exploited the failure of the *B. subtilis* SpoVID LysM domain to complement *C. difficile* LysM domain function (Fig. 4), we identified two point mutations in the LysM domain, W457E and I463R, that decrease heat-resistant spore formation by decreasing or even preventing binding to SpoIVA (Fig. 5). While these mutations reduced spore formation by \sim 100- and 10-fold, respectively, their effects on coat mislocalization were qualitatively less severe. The coat in *sipL* $_{\text{W457E/D/A}}$ and *sipL* $_{\text{I463R}}$ mutants appeared more closely associated with the forespore in these strains, particularly if the forespores/sporelets appeared phase bright (Fig. 5C). In contrast, the coat appeared to be more frequently displaced to the mother cell cytosol in *sipL* mutants carrying nonfunctional *sipL* alleles, such as the Δ_{lysM} , *sipL* $_{\Delta_{\text{I463R}}}$, and *sipL*-*lysM* $_{\text{Bsub}}$ (expressing *B. subtilis lysM*) strains (Fig. 1 and 5; see also Fig. S2 in the supplemental material). Indeed, the *sipL* strains that failed to produce heat-resistant spores did not make the phase-bright, swollen sporelets observed in the *sipL* $_{\text{W457E/D/A}}$ and *sipL* $_{\text{I463R}}$ mutants (Fig. 5C, purple arrows). It would be interesting to test whether the *sipL* $_{\text{W457E/D/A}}$ and *sipL* $_{\text{I463R}}$ mutants localize coat close to the forespore because the SipL $_{\text{W457E/D/A}}$ and SipL $_{\text{I463R}}$ variants can still localize to the forespore and/or partially encase the forespore. This scenario seems possible for the *sipL* $_{\text{W457E}}$ allele, since SipL $_{\text{W457E}}$ partially binds SpoIVA (Fig. 5D).

Our analyses also implicated the first residue of the LysM domain as being important for SipL function. The I463R mutation, but not the I463M or I463E mutation, significantly impaired SipL function while deletion of the Ile463 residue altogether completely abrogated SipL function (Fig. 5). These observations suggest that Ile463 is needed as a linker between the LysM domain and the rest of the SipL protein, or it could be needed for proper folding of the LysM domain. The latter possibility seems less likely, given that Ile463 is not strongly conserved at this position across LysM domains (Fig. S5) and does not appear to play an important structural role in the LysM domains whose structures have been solved (35).

LysM domains frequently bind to *N*-acetylglucosamine (NAG) residues in chitin (e.g., in eukaryotic LysM domains) and peptidoglycan in prokaryotic LysM-containing proteins (35, 36). Recent structural analyses have revealed the molecular basis for LysM binding to peptidoglycan (36). Interestingly, some of the residues identified as being critical for recognizing NAG in an *Enterococcus faecalis* LysM domain are not conserved in the four clostridial SipL $_{\text{LysM}}$ domains analyzed in this study (Fig. S5A, red asterisks) although they typically have similar properties in clostridial LysM domains. Nevertheless, when the structure of the *C. difficile* SipL $_{\text{LysM}}$ domain is predicted using the iTasser algorithm (37), it aligns closely with the structures of several LysM domains (Fig. S5B), raising the possibility that SipL $_{\text{LysM}}$ domains can bind peptidoglycan.

While this possibility remains to be tested, we note that the *B. subtilis* SpoVID $_{\text{LysM}}$ domain does not bind peptidoglycan even though putative peptidoglycan-binding

residues are conserved (32). In contrast, the LysM domain of SafA, a coat-morphogenetic protein that modulates inner coat assembly downstream of SpoVID (38, 39), functions both as a protein-protein interaction module and a peptidoglycan binding domain (32). Specifically, SafA's LysM domain binds to SpoVID early during coat morphogenesis while later during morphogenesis SafA's LysM domain binds to the spore cortex, the modified peptidoglycan layer that confers heat resistance to spores (32). Thus, even though SafA lacks a transmembrane domain to span the outer forespore membrane, its N-terminal LysM domain apparently binds the spore cortex, since SafA exhibits aberrant localization in cortex biogenesis mutants (32). It remains unclear how SafA binding switches from SpoVID to the cortex during spore formation, but a similar event would need to occur if *C. difficile* SipL's LysM domain binds SpoIVA and then to the cortex region. Directly testing whether clostridial SipL_{LysM} domains can bind peptidoglycan would provide important insight to these questions.

Interestingly, in the structure model generated by iTasser (Fig. S5B), the Trp457 residue we identified as being important for SipL to bind SpoIVA (Fig. S5B) is predicted to be surface exposed. Thus, Trp457 would appear to be available to directly interact with as-yet-undefined regions of SpoIVA and possibly also to bind cortex peptidoglycan. Future studies directed at identifying regions with SpoIVA that mediate binding to SipL will provide important insight into how the interaction between these two proteins allows for functional spore formation. Given that our results indicate that SpoIVA encasement of the forespore (Fig. 6) depends on SipL, it is possible that SipL binding to SpoIVA promotes SpoIVA polymerization. Alternatively, reduced levels of mCherry-SpoIVA in the $\Delta sipL$ strain may prevent self-polymerization of SpoIVA (40) and, thus, prevent encasement. Determining the precise effects of SipL binding to SpoIVA on SpoIVA's presumed ATPase and polymerization activities will provide critical insight into how infectious *C. difficile* spores are built and could guide efforts to prevent spore formation by clostridial pathogens.

MATERIALS AND METHODS

Bacterial strains and growth conditions. 630 $\Delta erm \Delta pyrE$ (28) was used as the parental strain for *pyrE*-based allele-coupled exchange (ACE) (28). *C. difficile* strains are listed in Table S1 in the supplemental material and were grown on supplemented brain heart infusion (BHIS) agar (41) supplemented with taurocholate (TA; 0.1%, wt/vol; 1.9 mM), kanamycin (50 $\mu\text{g}/\text{ml}$), and cefoxitin (8 $\mu\text{g}/\text{ml}$) as needed for conjugations. *C. difficile* defined medium (CDDM) (42) was used for isolating complementation strains (28). 5-Fluoroorotic acid (5-FOA) at 2 mg/ml and uracil at 5 $\mu\text{g}/\text{ml}$ were used as needed for ACE. Cultures were grown under anaerobic conditions using a gas mixture containing 85% N₂, 5% CO₂, and 10% H₂.

Escherichia coli strains for HB101/pRK24-based conjugations and BL21(DE3)-based protein production are listed in Table S1. *E. coli* strains were grown at 37°C, with shaking at 225 rpm in Luria-Bertani (LB) broth. The medium was supplemented with chloramphenicol (20 $\mu\text{g}/\text{ml}$) and ampicillin (50 $\mu\text{g}/\text{ml}$) as needed.

***E. coli* strain construction.** All primers are listed in Table S2, and all gBlocks used for cloning are listed in Table S3. Details of *E. coli* strain construction are provided in Text S1. All plasmid constructs were cloned into DH5 α , and sequence was confirmed using Genewiz. Plasmids to be conjugated into *C. difficile* were transformed into HB101/pRK24, while the plasmid used for antibody production was transformed into BL21(DE3).

***C. difficile* strain complementation.** Allele-coupled exchange (ACE) (28) was used as previously described (43) to construct the $\Delta spoIVA \Delta sipL \Delta pyrE$ mutant. The $\Delta spoIVA \Delta pyrE$ strain was used as the parental strain, with strain 1704 pMTL-YN3 $\Delta sipL$ being used to introduce the *sipL* mutation. pMTL-YN1C-based complementation constructs were conjugated into the $\Delta sipL \Delta pyrE$ strain as previously described (43). Two independent clones of each complementation strain were phenotypically characterized.

Plate-based sporulation. *C. difficile* strains were grown from glycerol stocks overnight on BHIS plates containing TA (0.1%, wt/vol). Colonies from these cultures were then used to inoculate liquid BHIS cultures, which were grown to stationary phase and then back-diluted 1:50 into BHIS medium. When the cultures reached an optical density at 600 nm (OD₆₀₀) between 0.35 and 0.7, 120 μl was removed to inoculate 70:30 agar plates (25). Sporulation was induced on this medium for 20 to 24 h. The ~20-h time point was used to analyze cultures by phase-contrast microscopy and harvest samples for Western blot analyses.

Heat resistance assay on sporulating cells. Heat-resistant spore formation was measured in sporulating *C. difficile* cultures after 20 to 24 h as previously described (44). Briefly, sporulating cultures were divided into two, with one culture being heat treated at 60°C for 30 min while the second half was left untreated. The samples were serially diluted and plated on BHIS-TA medium, and the heat resistance (HR) efficiency was calculated from the colonies that arose. Specifically, the HR efficiency represents the average ratio of heat-resistant cells for a given strain relative to the average ratio determined for the wild

type based on a minimum of three biological replicates. Statistical significance was determined using one-way analysis of variance (ANOVA) and Tukey's test.

Antibody production. The anti-SipL_{ΔLysM} antibody used in this study was raised against SipL_{ΔLysM}-His₆ in a rabbit by Cocalico Biologicals (Reamstown, PA). The recombinant protein was purified from *E. coli* strain 764 (25) (Table S1) using Ni²⁺-affinity resin as previously described (45).

TEM analyses. Sporulating cultures (23 h) were fixed and processed for electron microscopy by the University of Vermont Microscopy Center as previously described (25). A minimum of 50 full-length sporulating cells was used for phenotype counting.

Immunoprecipitation analyses. Sporulation was induced on 70:30 plates for 24 h as described above. Cultures from each of three 70:30 plates per strain were scraped into 1 ml of FLAG immunoprecipitation buffer (FIB; 50 mM Tris, pH 7.5, 150 mM NaCl, 0.02% sodium azide, 1× Halt protease inhibitor [ThermoScientific]). The cultures were transferred into tubes containing an ~300 μl of 0.1-mm zirconia-silica beads (BioSpec). The cultures were lysed using a FastPrep-24 instrument (MP Biomedicals) four times for 60 s each time at 5.5 M/s, with 5 min of cooling on ice between lysis intervals. The tubes were pelleted at 14,500 × *g* for 10 min at 4°C to pellet beads, unbroken cells/spores, and insoluble material. After the tubes were washed with additional FIB, the lysates were pooled, and FLAG-conjugated magnetic resin was added. This magnetic resin was generated by incubating Dynabead protein G (ThermoScientific) with anti-FLAG antibodies (Sigma-Aldrich) at room temperature followed by washing. The lysates were incubated with the anti-FLAG resin for 2 h at room temperature with rotation. After the beads were washed with FIB, FLAG-tagged proteins were eluted using FIB containing 0.1 mg/ml FLAG peptide (Sigma-Aldrich). All immunoprecipitations were performed on three independent biological replicates.

mCherry fluorescence microscopy. Live-cell fluorescence microscopy was performed using Hoechst 33342 (15 μg/ml; Molecular Probes) and mCherry protein fusions. Samples were prepared on agarose pads as previously described (30), and samples were imaged 30 min after harvesting to allow for mCherry fluorescence signal reconstitution in the anaerobically grown bacteria as previously described (27). Briefly, phase-contrast and fluorescence microscopy were performed using a Nikon 60× oil immersion objective (1.4 numerical aperture [NA]) on a Nikon 90i epifluorescence microscope. A CoolSnap HQ camera (Photometrics) was used to acquire multiple fields for each sample in 12-bit format using NIS-Elements software (Nikon). The Texas red channel was used to acquire images after a 3- to 90-ms exposure (90 ms for SipL-mCherry and mCherry-IVA, 50 ms for Hoechst staining, and ~3 ms for phase-contrast microscopy) with 2-by-2 binning. Images (10 Mhz) were subsequently imported into Adobe Photoshop CC 2015 for minimal adjustments in brightness/contrast levels and pseudocoloring. Localization analyses were performed on three independent biological replicates.

Western blot analyses. Samples for Western blotting were prepared as previously described (25). Briefly, sporulating cell pellets were resuspended in 100 μl of phosphate-buffered saline (PBS), and 50-μl samples were freeze-thawed for three cycles and then resuspended in 100 μl EBB buffer (8 M urea, 2 M thiourea, 4% [wt/vol] SDS, 2% [vol/vol] β-mercaptoethanol). The samples were boiled for 20 min, pelleted, resuspended in the same buffer to maximize protein solubilization, boiled for another 5 min, and then pelleted. Samples were resolved on 12% SDS-PAGE gels, transferred to Immobilon-FL polyvinylidene difluoride (PVDF) membrane, blocked in Odyssey blocking buffer with 0.1% (vol/vol) Tween 20. Rabbit anti-SipL_{ΔLysM} and mouse anti-SpoIVA (46) were used at 1:2,500 dilutions, rabbit anti-mCherry (Abcam) was used at a 1:2,000 dilution, and rabbit or mouse anti-Spo0A (25, 31) was used at a 1:1,000 dilution. IRDye 680CW and 800CW infrared dye-conjugated secondary antibodies were used at a minimum of a 1:25,000 dilution, and blots were imaged on an Odyssey LiCor CLx. Western blotting was performed on sporulating samples derived from three independent biological replicates.

SUPPLEMENTAL MATERIAL

Supplemental material for this article may be found at <https://doi.org/10.1128/JB.00042-19>.

SUPPLEMENTAL FILE 1, PDF file, 5.3 MB.

ACKNOWLEDGMENTS

We thank N. Bishop and J. Schwarz for excellent assistance in preparing samples for transmission electron microscopy throughout this study, D. Weiss and C. Ellermeier for providing the codon-optimized mCherry construct (47), A. Camilli for access to the Nikon microscope, N. Minton (University of Nottingham) for generously providing us with access to the 630 *Δerm ΔpyrE* strain and pMTL-YN1C and pMTL-YN3 plasmids for allele-coupled exchange (ACE), and M. Dembek for directly providing these materials to us and sharing his specific protocols on ACE.

Research in this paper was funded by award number T32AI007329 to M.H.T. and by R01AI22232 from the National Institutes of Allergy and Infectious Disease (NIAID) to A.S. A.S. is a Pew Scholar in the Biomedical Sciences supported by The Pew Charitable Trusts and a Burroughs Wellcome Investigator in the Pathogenesis of Infectious Disease supported by the Burroughs Wellcome Fund.

The content is solely the responsibility of the author(s) and does not necessarily

reflect the views of the Pew Charitable Trusts, Burroughs Wellcome, NIAID, or the National Institutes of Health. The funders had no role in study design, data collection and interpretation, or the decision to submit the work for publication.

A.S. has a paid consultancy for BioVector, Inc., a diagnostic start-up.

REFERENCES

- Freeman J, Bauer M, Baines S, Corver J, Fawley W, Goorhuis B, Kuijper E, Wilcox M. 2010. The changing epidemiology of *Clostridium difficile* infections. *Clin Microbiol Rev* 23:529–549. <https://doi.org/10.1128/CMR.00082-09>.
- Lessa FC, Mu Y, Bamberg WM, Beldavs ZG, Dumyati GK, Dunn JR, Farley MM, Holzbauer SM, Meek JI, Phipps EC, Wilson LE, Winston LG, Cohen JA, Limbago BM, Fridkin SK, Gerding DN, McDonald LC. 2015. Burden of *Clostridium difficile* infection in the United States. *N Engl J Med* 372:825–834. <https://doi.org/10.1056/NEJMoa1408913>.
- Deakin LJ, Clare S, Fagan RP, Dawson LF, Pickard DJ, West MR, Wren BW, Fairweather NF, Dougan G, Lawley TD. 2012. The *Clostridium difficile* *spo0A* gene is a persistence and transmission factor. *Infect Immun* 80:2704–2711. <https://doi.org/10.1128/IAI.00147-12>.
- Dembek M, Willing SE, Hong HA, Hosseini S, Salgado PS, Cutting SM. 2017. Inducible expression of *spo0A* as a universal tool for studying sporulation in *Clostridium difficile*. *Front Microbiol* 8:1793. <https://doi.org/10.3389/fmicb.2017.01793>.
- Paredes-Sabja D, Shen A, Sorg JA. 2014. *Clostridium difficile* spore biology: sporulation, germination, and spore structural proteins. *Trends Microbiol* 22:406–416. <https://doi.org/10.1016/j.tim.2014.04.003>.
- Chandrasekaran R, Lacy DB. 2017. The role of toxins in *Clostridium difficile* infection. *FEMS Microbiol Rev* 41:723–750. <https://doi.org/10.1093/fems/rev/fux048>.
- Jump RL, Pultz MJ, Donskey CJ. 2007. Vegetative *Clostridium difficile* survives in room air on moist surfaces and in gastric contents with reduced acidity: a potential mechanism to explain the association between proton pump inhibitors and *C. difficile*-associated diarrhea? *Antimicrob Agents Chemother* 51:2883–2887. <https://doi.org/10.1128/AAC.01443-06>.
- Koenigsnecht MJ, Theriot CM, Bergin IL, Schumacher CA, Schloss PD, Young VB. 2015. Dynamics and establishment of *Clostridium difficile* infection in the murine gastrointestinal tract. *Infect Immun* 83:934–941. <https://doi.org/10.1128/IAI.02768-14>.
- Tan IS, Ramamurthi KS. 2014. Spore formation in *Bacillus subtilis*. *Environ Microbiol Rep* 6:212–225. <https://doi.org/10.1111/1758-2229.12130>.
- Driks A, Eichenberger P. 2016. The Spore Coat. *Microbiol Spectr* 4:TBS-0023-2016. <https://doi.org/10.1128/microbiolspec.TBS-0023-2016>.
- Setlow P. 2014. Germination of spores of *Bacillus* species: what we know and do not know. *J Bacteriol* 196:1297–1305. <https://doi.org/10.1128/JB.01455-13>.
- McKenney PT, Driks A, Eichenberger P. 2013. The *Bacillus subtilis* endospore: assembly and functions of the multilayered coat. *Nat Rev Microbiol* 11:33–44. <https://doi.org/10.1038/nrmicro2921>.
- Gill RL, Jr, Castaing JP, Hsin J, Tan IS, Wang X, Huang KC, Tian F, Ramamurthi KS. 2015. Structural basis for the geometry-driven localization of a small protein. *Proc Natl Acad Sci U S A* 112:E1908. <https://doi.org/10.1073/pnas.1423868112>.
- Ramamurthi KS, Clapham KR, Losick R. 2006. Peptide anchoring spore coat assembly to the outer forespore membrane in *Bacillus subtilis*. *Mol Microbiol* 62:1547–1557. <https://doi.org/10.1111/j.1365-2958.2006.05468.x>.
- Ramamurthi KS, Losick R. 2008. ATP-driven self-assembly of a morphogenetic protein in *Bacillus subtilis*. *Mol Cell* 31:406–414. <https://doi.org/10.1016/j.molcel.2008.05.030>.
- McKenney PT, Eichenberger P. 2012. Dynamics of spore coat morphogenesis in *Bacillus subtilis*. *Mol Microbiol* 83:245–260. <https://doi.org/10.1111/j.1365-2958.2011.07936.x>.
- Wang KH, Isidro AL, Domingues L, Eskandarian HA, McKenney PT, Drew K, Grabowski P, Chua MH, Barry SN, Guan M, Bonneau R, Henriques AO, Eichenberger P. 2009. The coat morphogenetic protein SpoVID is necessary for spore encasement in *Bacillus subtilis*. *Mol Microbiol* 74:634–649. <https://doi.org/10.1111/j.1365-2958.2009.06886.x>.
- Roels S, Driks A, Losick R. 1992. Characterization of *spoIVA*, a sporulation gene involved in coat morphogenesis in *Bacillus subtilis*. *J Bacteriol* 174:575–585. <https://doi.org/10.1128/jb.174.2.575-585.1992>.
- Beall B, Driks A, Losick R, Moran CP, Jr. 1993. Cloning and characterization of a gene required for assembly of the *Bacillus subtilis* spore coat. *J Bacteriol* 175:1705–1716. <https://doi.org/10.1128/jb.175.6.1705-1716.1993>.
- Levin PA, Fan N, Ricca E, Driks A, Losick R, Cutting S. 1993. An unusually small gene required for sporulation by *Bacillus subtilis*. *Mol Microbiol* 9:761–771. <https://doi.org/10.1111/j.1365-2958.1993.tb01736.x>.
- Tan IS, Weiss CA, Popham DL, Ramamurthi KS. 2015. A quality-control mechanism removes unfit cells from a population of sporulating bacteria. *Dev Cell* 34:682–693. <https://doi.org/10.1016/j.devcel.2015.08.009>.
- Fernandes CG, Moran CP, Jr, Henriques AO. 2018. Autoregulation of SafA assembly through recruitment of a protein cross-linking enzyme. *J Bacteriol* 200:e00066-18. <https://doi.org/10.1128/JB.00066-18>.
- Galperin MY, Mekhedov SL, Puigbo P, Smirnov S, Wolf YI, Rigden DJ. 2012. Genomic determinants of sporulation in Bacilli and Clostridia: towards the minimal set of sporulation-specific genes. *Environ Microbiol* 14:2870–2890. <https://doi.org/10.1111/j.1462-2920.2012.02841.x>.
- Henriques AO, Moran CP, Jr. 2007. Structure, assembly, and function of the spore surface layers. *Annu Rev Microbiol* 61:555–588. <https://doi.org/10.1146/annurev.micro.61.080706.093224>.
- Putnam EE, Nock AM, Lawley TD, Shen A. 2013. SpoIVA and Sipl are *Clostridium difficile* spore morphogenetic proteins. *J Bacteriol* 195:1214–1225. <https://doi.org/10.1128/JB.02181-12>.
- Ribis JW, Ravichandran P, Putnam EE, Pishdadian K, Shen A. 2017. The conserved spore coat protein SpoVM is largely dispensable in *Clostridium difficile* Spore Formation. *mSphere* 2:e00315-17. <https://doi.org/10.1128/mSphere.00315-17>.
- Ribis JW, Fimlaid KA, Shen A. 2018. Differential requirements for conserved peptidoglycan remodeling enzymes during *Clostridioides difficile* spore formation. *Mol Microbiol* 110:370–389. <https://doi.org/10.1111/mmi.14090>.
- Ng YK, Ehsaan M, Philip S, Collery MM, Janoir C, Collignon A, Cartman ST, Minton NP. 2013. Expanding the repertoire of gene tools for precise manipulation of the *Clostridium difficile* genome: allelic exchange using *pyrE* alleles. *PLoS One* 8:e56051. <https://doi.org/10.1371/journal.pone.0056051>.
- Collery MM, Kuehne SA, McBride SM, Kelly ML, Monot M, Cockayne A, Dupuy B, Minton NP. 2016. What's a SNP between friends: the influence of single nucleotide polymorphisms on virulence and phenotypes of *Clostridium difficile* strain 630 and derivatives. *Virulence* 8:767–781. <https://doi.org/10.1080/21505594.2016.1237333>.
- Fimlaid KA, Jensen O, Donnelly ML, Siegrist MS, Shen A. 2015. Regulation of *Clostridium difficile* spore formation by the SpoIQ and SpoIIA proteins. *PLoS Genet* 11:e1005562. <https://doi.org/10.1371/journal.pgen.1005562>.
- Fimlaid KA, Bond JP, Schutz KC, Putnam EE, Leung JM, Lawley TD, Shen A. 2013. Global analysis of the sporulation pathway of *Clostridium difficile*. *PLoS Genet* 9:e1003660. <https://doi.org/10.1371/journal.pgen.1003660>.
- Pereira FC, Nunes F, Cruz F, Fernandes C, Isidro AL, Lousa D, Soares CM, Moran CP, Jr, Henriques AO, Serrano M. 2019. A LysM domain intervenes in sequential protein-protein and protein-peptidoglycan interactions important for spore coat assembly in *Bacillus subtilis*. *J Bacteriol* 201:e00642-18. <https://doi.org/10.1128/JB.00642-18>.
- Yutin N, Galperin MY. 2013. A genomic update on clostridial phylogeny: Gram-negative spore formers and other misplaced clostridia. *Environ Microbiol* 15:2631–2641. <https://doi.org/10.1111/1462-2920.12173>.
- Sasi Jyothsna TS, Tushar L, Sasikala C, Ramana CV. 2016. *Paraclostridium benzoelyticum* gen. nov., sp. nov., isolated from marine sediment and reclassification of *Clostridium bifermentans* as *Paraclostridium bifermentans* comb. nov. Proposal of a new genus *Paeniclostridium* gen. nov. to accommodate *Clostridium sordellii* and *Clostridium ghanii*. *Int J Syst Evol Microbiol* 66:1268–1274. <https://doi.org/10.1099/ijsem.0.000874>.
- Dworkin J. 2018. Detection of fungal and bacterial carbohydrates: do the similar structures of chitin and peptidoglycan play a role in immune dysfunction? *PLoS Pathog* 14:e1007271. <https://doi.org/10.1371/journal.ppat.1007271>.
- Mesnage S, Dellarole M, Baxter NJ, Rouget JB, Dimitrov JD, Wang N, Fujimoto Y, Hounslow AM, Lacroix-Desmazes S, Fukase K, Foster SJ,

- Williamson MP. 2014. Molecular basis for bacterial peptidoglycan recognition by LysM domains. *Nat Commun* 5:4269. <https://doi.org/10.1038/ncomms5269>.
37. Yang J, Yan R, Roy A, Xu D, Poisson J, Zhang Y. 2015. The I-TASSER suite: protein structure and function prediction. *Nat Methods* 12:7–8. <https://doi.org/10.1038/nmeth.3213>.
38. Ozin A, Samford C, Henriques A, Moran C. 2001. SpoVID guides SafA to the spore coat in *Bacillus subtilis*. *J Bacteriol* 183:3041–3049. <https://doi.org/10.1128/JB.183.10.3041-3049.2001>.
39. Ozin AJ, Henriques AO, Yi H, Moran CP, Jr. 2000. Morphogenetic proteins SpoVID and SafA form a complex during assembly of the *Bacillus subtilis* spore coat. *J Bacteriol* 182:1828–1833. <https://doi.org/10.1128/JB.182.7.1828-1833.2000>.
40. Castaing J-P, Nagy A, Anantharaman V, Aravind L, Ramamurthi K. 2013. ATP hydrolysis by a domain related to translation factor GTPases drives polymerization of a static bacterial morphogenetic protein. *Proc Natl Acad Sci USA* 110:E151–E160. <https://doi.org/10.1073/pnas.1210554110>.
41. Sorg JA, Dineen SS. 2009. Laboratory maintenance of *Clostridium difficile*. *Curr Protoc Microbiol* Chapter 9:Unit 9A1. <https://doi.org/10.1002/9780471729259.mc09a01s12>.
42. Karasawa T, Ikoma S, Yamakawa K, Nakamura S. 1995. A defined growth medium for *Clostridium difficile*. *Microbiology* 141:371–375. <https://doi.org/10.1099/13500872-141-2-371>.
43. Donnelly ML, Li W, Li YQ, Hinkel L, Setlow P, Shen A. 2017. A *Clostridium difficile*-specific, gel-forming protein required for optimal spore germination. *mBio* 8:e02085-16. <https://doi.org/10.1128/mBio.02085-16>.
44. Shen A, Fimlaid KA, Pishdadian K. 2016. Inducing and quantifying *Clostridium difficile* spore formation. *Methods Mol Biol* 1476:129–142. https://doi.org/10.1007/978-1-4939-6361-4_10.
45. Adams CM, Eckenroth BE, Putnam EE, Doublet S, Shen A. 2013. Structural and functional analysis of the CspB protease required for *Clostridium* spore germination. *PLoS Pathog* 9:e1003165. <https://doi.org/10.1371/journal.ppat.1003165>.
46. Kevorkian Y, Shirley DJ, Shen A. 2016. Regulation of *Clostridium difficile* spore germination by the CspA pseudoprotease domain. *Biochimie* 122:243–254. <https://doi.org/10.1016/j.biochi.2015.07.023>.
47. Ransom EM, Ellermeier CD, Weiss DS. 2015. Use of mCherry red fluorescent protein for studies of protein localization and gene expression in *Clostridium difficile*. *Appl Environ Microbiol* 81:1652–1660. <https://doi.org/10.1128/AEM.03446-14>.
48. Pogliano J, Osborne N, Sharp MD, Abanes-De Mello A, Perez A, Sun YL, Pogliano K. 1999. A vital stain for studying membrane dynamics in bacteria: a novel mechanism controlling septation during *Bacillus subtilis* sporulation. *Mol Microbiol* 31:1149–1159. <https://doi.org/10.1046/j.1365-2958.1999.01255.x>.